Available online at www.sciencedirect.com
SCIENCE DIRECT®
Journal of Power Sources 133 (2004) 214–222
JOURNAL OF POWER SOURCES
www.elsevier.com/locate/jpowsour

Evaluation of a sol–gel process for the synthesis of $La_{1-x}Sr_xMnO_{3+\delta}$ cathodic multilayers for solid oxide fuel cells

Manuel Gaudon [a], Christel Laberty-Robert [a], Florence Ansart [a,*], Laurent Dessemond [b], Philippe Stevens [c]

[a] *CIRIMAT/LCMIE, Université Paul Sabatier, Bat II R1, 118 Route de Narbonne, 31062 Toulouse Cedex 4, France*
[b] *LEPMI, INP Grenoble, BP 75, 38402 Saint Martin d'Hères Cedex, France*
[c] *EDF, European Institut for Energy Research, Universität Karlsruhe, Adenauerring 20, D-76131 Karlsruhe, Germany*

Received 19 September 2003; received in revised form 12 February 2004; accepted 16 February 2004

Abstract

Solid oxide fuel cells (SOFCs) are electrical energy conversion devices with high efficiency and low pollution. In order to increase performances of SOFCs at intermediate temperature (700–800 °C) and to decrease materials cost, an alternative sol–gel synthesis method has been investigated to deposit $La_{1-x}Sr_xMnO_{3+\delta}$ (LSM*x*) as cathode thin films. Polycrystalline LSM*x* thin films were prepared by dip-coating using a polymeric solution. Lanthanum, strontium and manganese nitrates were used as raw materials. The viscosity of the solution was adjusted and the solution was deposited on polycrystalline ZrO_2–8% Y_2O_3 ceramics. Prior to experiments, the substrate surface was eroded until a roughness of 20 nm and then cleaned with ethanol and dried. Film thicknesses were adjusted with the number of layers. Porosity and grain size of monolayers or multilayers were evaluated. Typical thickness of monolayer is 250 nm. A key parameter in the multilayer process was the intermediate calcination temperature (400, 700 or 1000 °C) of each further layer deposition. A correlation between this intermediate temperature and morphology, thickness and porosity was found; porosity is ranging from 3 to 40% and thickness can reach 1 micron for multilayers. Concerning electrochemical performances, the best results were obtained for LSM0.4 multilayers with an intermediate calcination temperature (called T_i) of 400 °C.

Keywords: Cathodic multilayers; Solid oxide fuel cells; Sol–gel process; Electrochemical performances

1. Introduction

Solid oxide fuel cells (SOFCs) are energy conversion devices with high efficiency (≈70%) and low pollution compared with conventional electric generation methods [1,2]. Nevertheless, in order to develop industrial applications of such systems, it is necessary to reduce their operating temperatures. Lowering SOFC operating temperatures allows a reduction of stack insulation requirements and increases cell life because of reduced thermal cycling stress. Now, the decrease of the working temperature is in part limited by the cells cathodic overpotentials. The increase of the interfacial resistances can be overcome by finding a new electrode material with high electrochemical reaction rate [3–6]. The difficulties due to lower interfacial resistances can be also solved by increasing the number of reactive sites at the interface. A solution is to prepare porous thin films of conventional LSM*x* oxides on dense electrolyte (YSZ). The aim of this paper is to optimize the microstructure of thin films of $La_{1-x}Sr_xMnO_{3+\delta}$ (LSM*x* with *x* strontium content) prepared by a polymeric route, which is a low cost synthesis method [7,8]. Indeed, it is now well established that the performances of LSM*x*-based cathodes deposited on YSZ pellets are affected not only by the chemical composition of electrodes but also by the microstructure of the electrodes [9–12]. Thin films with different microstructures and thicknesses were elaborated by varying the sol parameters (viscosity, dip-coating speed, etc.). Films morphologies are correlated with electric and electrochemical properties. Results allow a better understanding of cathodes electrochemical properties. Then, the advantages and the limits of such elaboration process will be discussed.

* Corresponding author. Tel.: +33-5-61-556108; fax: +33-5-61-556163.
E-mail address: ansart@chimie.ups-tlse.fr (F. Ansart).

0378-7753/$ – see front matter © 2004 Elsevier B.V. All rights reserved.
doi:10.1016/j.jpowsour.2004.02.019

2. Experimental

2.1. Thin films elaboration

Lanthanum, strontium and manganese nitrates were used as raw materials. Nitrates in the LSM*x* stoechiometric proportions were dissolved in acetic acid solution. Hexamethylenetetramine (HMTA) was dissolved in acetylacetone and acetic acid solution. These solutions were mixed together and the volume of the solution was adjusted to 400 mL by heating the solution at 80–90 °C. The synthesis parameters of the polymeric solution (viscosity, cationic salts concentration, etc.), the substrate surface roughness and the deposition method were described in a previous paper [13]. After deposition, each layer was dried in a furnace at about 100 °C to remove residual solvents. For multilayers synthesis, the heat treatment was carried out in two stages: intermediate heating at different temperatures (T_i = 400, 700 or 1000 °C) for 2 h at a heating rate of 100 °C h^{-1} followed thereafter by a final heating at a temperature (T_f) of 1000 °C. Each layer was heat-treated at T_i before the next layer was coated. This process was repeated several times before final heating. The choice of the calcination temperatures (T_i and T_f) will be discussed in Section 3.

To determine heat treatment conditions, the thermal decomposition of the gel under air was studied by differential thermal analysis (DTA) and thermogravimetric analysis (TGA). These analyses were made with a heating rate of 360 °C h^{-1} using a SETARAM 92B thermobalance (accuracy 10^{-4} g).

X-ray diffraction (XRD) patterns were obtained using a Cu Ka radiation (SIEMENS D501) source to analyze the films structure. The crystallite sizes of the powders were determined from X-ray diffraction line broadening using the Scherrer formula [14].

Scanning electron microscopy was used to study the microstructure of LSM*x* films. Films porosity and grain sizes were evaluated from image treatment of scanning electron micrographs. The thickness of the coated films was measured by a profilometer (Zygometer). A step was created by mechanical abrasion.

Transmission electron microscopy coupled with EDX analyses were used to study the substrate/thin films interface.

2.2. Electrical and electrochemical characterization

Electrical properties of thin films have been studied with a four probes device (Fig. 1a).

Electrochemical behavior of LSM0.4 films of different microstructures has been studied by means of impedance spectroscopy. Measurements were carried out on three-electrode electrochemical cells. A schematic of the investigated half cells is shown on Fig. 1b. The counter and reference electrodes were deposited by rf sputtering (Plassys) at room temperature on the reverse side of the YSZ substrate. A Pt grid, used as a current collector, was slightly pressed against the working electrode (LSM0.4 films). The current collection on both counter and reference electrodes was performed by using Pt wires pressed in contact on the sputtered layers. Impedance spectroscopy measurements were performed at open circuit potential, in air between 600 and 800 °C. The electrode characteristics were recorded with an Autolab potentiostat–galvanostat (Eco-Chemie) in the 104 to 10−3 Hz frequency range. The amplitude of the measuring signal was equal to 40 mV.

3. Results and discussion

3.1. Determination of heat treatment conditions

The microstructure of thin films obtained by a sol–gel process is known to be sensitive to the heat treatment. Thus, it is very important to determine the heating conditions before the preparation of thin films.

In this study, the heating conditions are determined by the decomposition behavior of LSM0.4 dried gels and XRD analyses of dried gels calcined at various temperatures.

The TGA and DTA results for the LSM04 precursors are shown in Fig. 2. The TG curve indicates a weight loss associated to the removal of adsorbed water and solvents from 100 to 270 °C. There is a large weight loss at 350 °C due to the decomposition of organic compounds of the precursor powder and this decomposition ends up at 400 °C. The exothermic peaks at 280 and at 350 °C related to the pre-

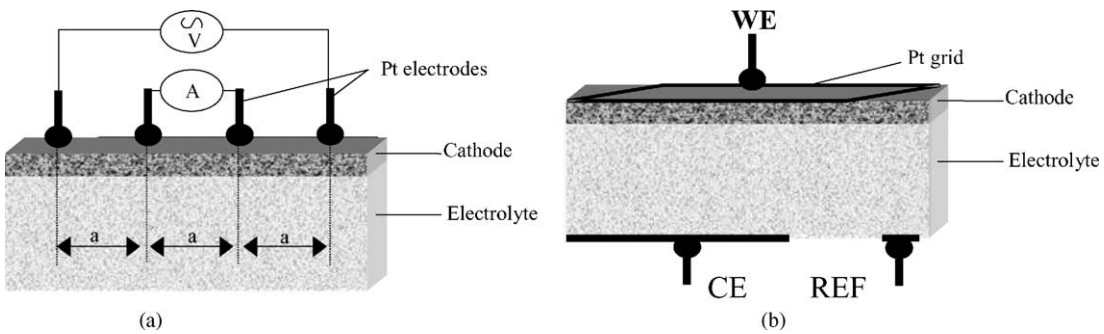

Fig. 1. Four probes device and three electrodes device for electrical (a) and electrochemical measurements (b).

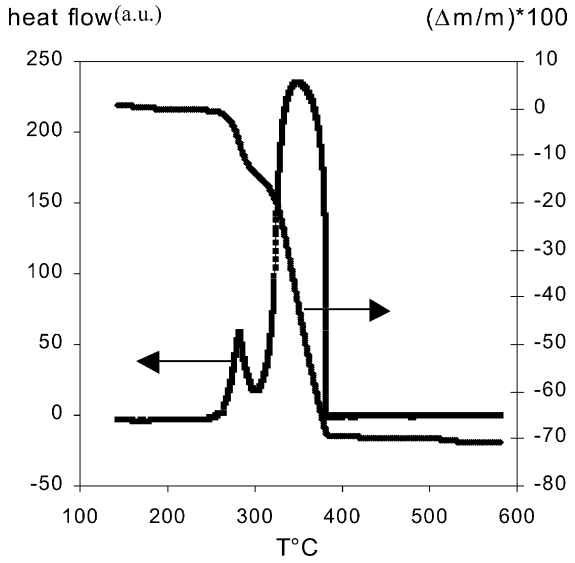

Fig. 2. TGA and DTA results for the LSM0.4 dried gel.

vious weight losses correspond to the decomposition of the dried gel.

XRD analyses are used to obtain more information on the decomposition behavior. The XRD patterns of the powders annealed at 400, 600, 700 and 1000 °C are shown in Fig. 3. A diffuse XRD pattern is observed at 400 °C, indicating the formation of an inorganic amorphous precursor after pyrolysis. For temperatures higher than 400 °C, the crystallization of the LSM0.4 perovskite phase begins. No intermediate phase is observed which suggests a direct crystallization from the amorphous phase. For a calcination temperature of 600 °C, several broad peaks appear. They can be attributed to the perovskite structure of LSM0.4 powders. However, when the calcination temperature increases, the peaks become much sharper, showing a better crystallinity of the

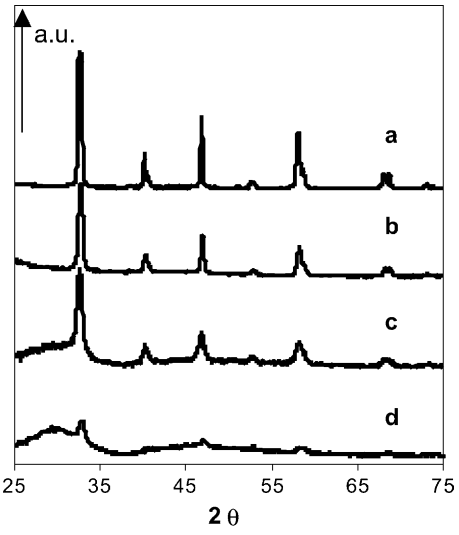

Fig. 3. XRD patterns of LSM0.4 powders annealed at: (a) 400 °C; (b) 600 °C; (c) 700 °C; and (d) 1000 °C.

powders. Good crystallinity is observed at a calcination temperature of 700 °C. The average grain size was determined from XRD patterns using Scherrer formula [14] and value is close to 35 nm. When the heating temperature increases from 700 to 1000 °C, the crystallite size of the LSM04 powders increases from 35 to 145 nm, showing a grain growth process.

In order to define the final heating temperature, the film/substrate interface was studied by TEM analyses coupled with EDX analyses. In Fig. 4, transmission electronic micrography of the LSM0/YSZ interface heat treated at 1200 °C during 2 h in air is reported. As it can be seen, such heat treatment produces a new layer above the perovskite grains. Electronic diffraction diagram coupled with EDX analysis shows the presence of $La_2Zr_2O_7$ phase (Fig. 4b). This insulating compound is well known to decrease the performances of the electrochemical system [15–19].

According to TG and XRD analyses, three intermediate temperatures are chosen for the heating procedure during the multilayers synthesis. Whatever the intermediate temperature, according to film/substrate interface study, the final sintering temperature for multilayers is 1000 °C. $T_i = 400$ °C is chosen because it corresponds to the end of the pyrolysis of organic compounds. Then, experiments were done with $T_i = 700$ °C, because at this temperature, the powders are well crystallized. The average grain size is small and all organics have disappeared. To complete the study, $T_i = 1000$ °C is also used.

In the following section, the effect of the intermediate temperature will be studied on the microstructural properties (thickness, grain size and porosity) of the film.

3.2. Thin films characterization

Multilayers of LSM*x* with $x = 0, 0.2, 0.4$, and a number of layers (n) ranging from 1 to 5 were prepared. Three intermediate calcination temperatures T_i were used: 400, 700 and 1000 °C and whatever T_i, final temperature T_f is constant and equal to 1000 °C.

In Fig. 5, is reported the effect of strontium on monolayers LSM*x* morphology ($x = 0$, 0.2 and 0.4). It can be seen that the higher the strontium rate, the smaller the particles size. This result is the same, whatever n. A comparison between the grains size and the thickness shows that the monolayers are constituted of a single grains layer.

In Fig. 6, are presented LSM0.4 multilayers ($n = 3$ and 5) for three intermediate temperatures T_i. The grains size increases with n. The mean diameters (using about a hundred grains) and the porosity of the film were calculated in order to compare the effect of processing parameters on the film morphology. The results obtained are reported in Table 1 according to x, n and T_i. The thicknesses measured by optical profilometry are also reported in this table.

For $T_i = 400$ °C, the grains size strongly increases between $n = 1$ and 3. For $x = 0.4$, the mean grains size for $n = 1$ is 180 nm and for $n = 3$ is 330 nm. However, the

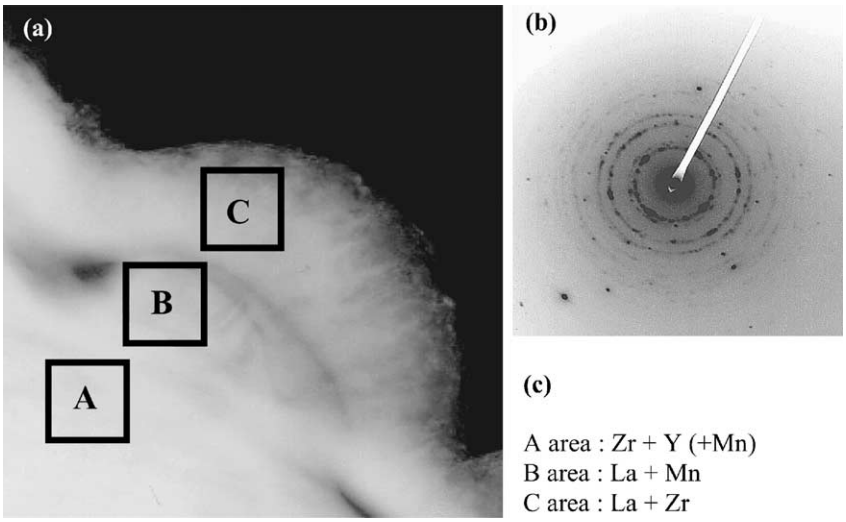

Fig. 4. (a) TEM micrograph of the interface between LSM0 and YSZ heat treated at 1200 °C; (b) electronic diffraction diagram of C area; (c) EDX analyses at points A, B and C.

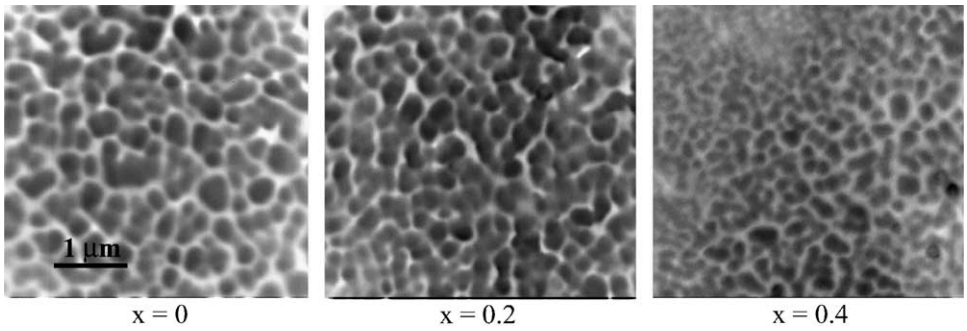

Fig. 5. SEM micrographs on three LSM*x* monolayers ($T_i = 1000\,^{\circ}C$).

porosity is quite the same, whatever *n*. This could explain linear evolution of thickness versus *n*. Indeed, the thickness of a five layers deposit (975 nm) is approximately equal to 5 nm × 200 nm (200 nm is the monolayer thickness).

Table 1
The grain mean diameter, the thickness and the porosity of LSM*x* multilayers according to *x*, *n* and T_i

	T_i (°C)	*x*	Mean diameter (in nm with ±10 nm)	Thickness (in nm with ±10 nm)	Porosity (in percentage with 10%)
1	–	0	265	230	40
	–	0.4	180	200	29
3	400	0	540	660	35
		0.4	330	575	28
	700	0	435	465	15
		0.4	290	560	18
	1000	0	350	610	32
		0.4	285	585	28
5	400	0	550	1080	34
		0.4	350	940	27
	700	0	550	687	3
		0.4	300	860	15
	1000	0	470	985	30
		0.4	275	975	28

For $T_i = 1000\,^{\circ}C$, the films microstructure is very similar to the ones observed for $T_i = 400\,^{\circ}C$. Only a slight increase of the grains size is obtained with *n*. Besides, porosity distribution is less homogeneous, particularly for high values of *n*. This phenomenon could be explained by a beginning of multilayers sintering for $T_i = 1000\,^{\circ}C$. Indeed, for $T_i = 1000\,^{\circ}C$, multilayers were heat treated at 1000 °C several times (corresponding to the number of layers).

For $T_i = 700\,^{\circ}C$, the main difference is an important decrease of films porosity with the number of layers. This densification is more important for $x = 0$ than for $x = 0.4$. For example, a five layers deposit is 15% porous for $x = 0.4$, but is only 3% porous for $x = 0$. Consequently, it is important to notice that this treatment leads to thinner films than the previous ones ($T_i = 400$ or $1000\,^{\circ}C$). In this case, the evolution of films thickness is not linear with *n*.

Morphology of final oxides allows an understanding of nucleation and growth steps mechanisms of LSM*x*. Mechanical abrasions show that grains anchorage to the substrate only begins at about 800 °C. So, a germination process beginning at the film/substrate interface can be excluded. In addition, the growth of the first crystallites is advantaged beside the formation of new crystallites. Indeed, monolayers consist of a single grains layer. The important porosity of

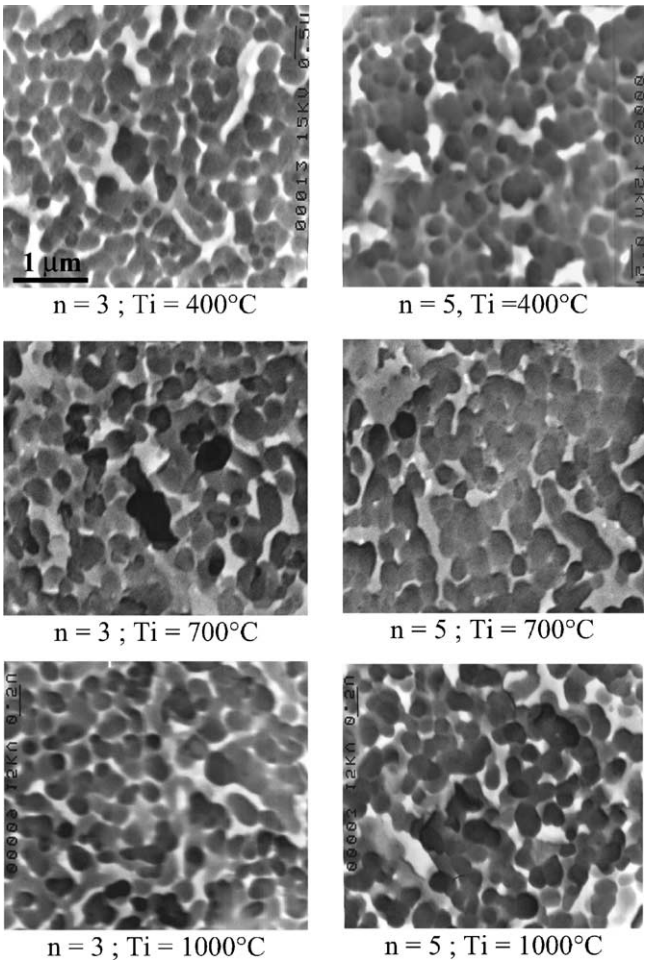

Fig. 6. SEM micrographs of LSM0.4 multilayers.

films synthesized by polymeric route is usually linked to the high quantity of organic compounds evaporated during calcination. In our case, it seems rather due to the grain growth. Indeed, this effect limits the elimination of the porosity during the final sintering.

For $T_i = 700\,^{\circ}C$, a densification is observed with n because this intermediate temperature is high enough to allow crystallites formation. However, it does not allow the crystallites growth. Then, during the final heating, the high number of crystallites present in the film allows a better volume densification.

3.3. Electrical characterization

The electrical tests have been performed in order to evaluate the samples elaborated by sol–gel process having the best conductivity.

3.3.1. Effect of film thickness on conductivity

The influence of the thickness (or n) on conductivity is studied and results are reported in Fig. 7. The activation energies and the conductivities at 800 °C, obtained by an extrapolation at high temperatures, for LSMx films with $x = 0.4$, $n = 1$, 3, and 5, are presented in Table 2. The electrical conductivity calculated at 800 °C for monolayer is smaller than for multilayers (for the monolayer: $\sigma = 1.5\,S\,cm^{-1}$, for the multilayer with $n = 3$: $\sigma = 15\,S\,cm^{-1}$). The activation energy for monolayer (0.24 eV) is bigger than the one observed for multilayer (0.14 eV). Different interpretations can be proposed: (i) thickness of a monolayer is too small to be characterized by a four probe device; (ii) the grain monolayers percolation is very poor; (iii) the grain size for a monolayer (grain size diameter = 180 nm) is smaller than that of multilayers (330 nm for $n = 3$, 350 nm for $n = 5$).

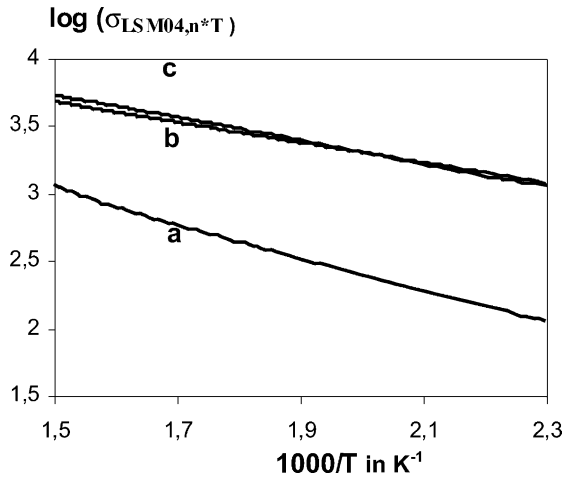

Fig. 7. Electronic conductivities as a function of temperature for LSM0.4 thin films for (a) $n = 1$; (b) $n = 3$; (c) $n = 5$.

A comparison of the activation energy and the electrical conductivity for multilayers shows that there is no film thickness dependence on the electrical properties for films thicker than 600 nm. The conductivity at 800 °C for $n = 3$ and 5 is the same, 15–16 $S\,cm^{-1}$. A microstructural study shows that the grain size is not very different for $n = 3$ and 5. The difference in activation energy and conductivity between monolayer and multilayers seems mostly due to a poor grain percolation for monolayer. Furthermore, similar results of conductivity for multilayers show that there is no improvement of grains percolation beyond films thicker than 600 nm ($n > 3$). However, the conductivity at 800 °C of LSM04 thin films is lower by a factor of 10 to the value of LSMx polycrystalline ceramic sample (σ varies between 100 and 200 $S\,cm^{-1}$, according to the strontium content [20–23]). These results suggest that the conductivity of our thin films is mostly determined by the conductivity of grain boundary (grain boundary effect).

Table 2
Activation energy and electrical conductivities at 800 °C for LSM04, n multilayers, $T_i = 400\,^{\circ}C$

n	E_a (eV)	σ at 800 °C ($S\,cm^{-1}$)
1	0.240	5
3	0.145	15
5	0.140	16

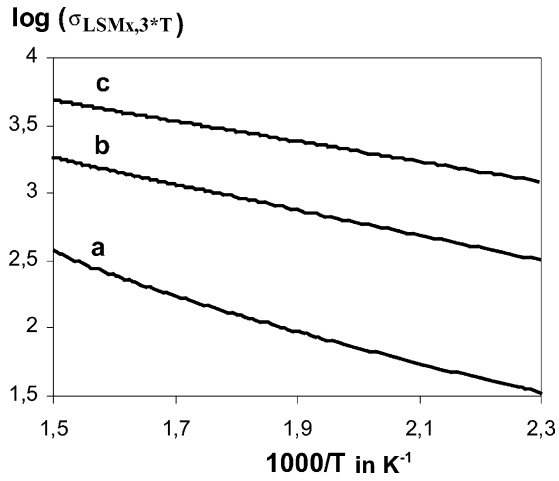

Fig. 8. Electronic conductivities as a function of temperature for LSM*x* thin films with $n = 3$ for (a) $x = 0$; (b) $x = 0.2$; (c) $x = 0.4$.

3.3.2. *Effect of strontium content on conductivity*

For $n = 3$, the effect of strontium content on electrical properties is studied and results are reported in Fig. 8. The activation energy and the conductivity at 800 °C, for LSM*x* films with $x = 0, 0.2$ and 0.4 are reported in Table 3. The polaron theory describes the electrical conduction in this perovskite oxides. It predicts a maximum of conductivity for a number of Mn^{3+}/Mn^{4+} couples maximum. This value can be calculated by the following ratio: $[Mn^{3+}][Mn^{4+}]/([Mn^{3+}] + [Mn^{4+}])^2$. The maximum of couple is observed when $[Mn^{3+}] = [Mn^{4+}]$, and when $r = [Mn^{3+}]/[Mn^{4+}] = 1$. The study of the stoechiometric level δ in these oxides [24] shows that the r ratio is close to 1 whatever the strontium content ($0 < x < 0.4$). For small strontium contents, a value of r close to 1 is explained by a high stoechiometric level δ [24]. In our samples, the conductivity increases with the strontium content as expected and the best result is observed for $x = 0.4$. However, the increase in the conductivity is very important, and a change in the conductivity by a factor of 10 is observed between $x = 0$ ($\sigma = 1.5\,S\,cm^{-1}$) and $x = 0.4$ ($\sigma = 15\,S\,cm^{-1}$). Thus, it seems that the conductivity depends on both the number of Mn^{3+}/Mn^{4+} couples and the materials microstructure (grain size, porosity and thickness [25]).

3.4. *Electrochemical characterization*

For electrochemical measurements, we consider the half-cell constituted by the substrate, the electrode and the current collector. The aim of this study is to evaluate by impedance spectroscopy the microstructure influence on the electrochemical properties of cathodes elaborated by sol–gel process. All impedance experimental spectra are normalized by the electrode/electrolyte contact surface unit. In terms of technological applications, perovskite-based materials used as a cathode in SOFC, must fulfill different criterions. In particular, electrolyte and overpotential resistances lower than 0.2 and $1\,W\,cm^2$, respectively, at 850 °C are expected in order to increase the performances of these electrochemical systems [26,27].

Table 3
Activation energy and electrical conductivities at 800 °C for LSM*x* multilayers with $n = 3$, $T_i = 400$ °C

x	E_a (eV)	σ at 800 °C ($S\,cm^{-1}$)
0	0.223	1.5
0.2	0.185	7
0.4	0.145	15

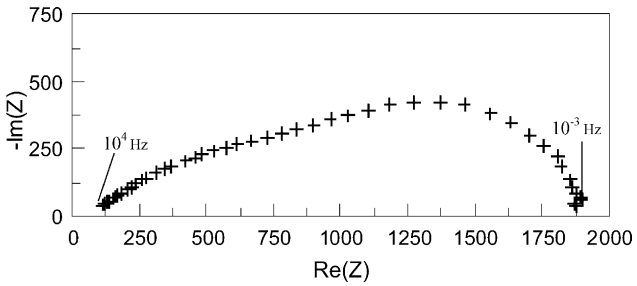

Fig. 9. Impedance diagram at 800 °C of a LSM04 monolayer with Pt grid as current collector.

The electrochemical behaviors of the multilayers electrodes (with $n = 3$ and 5, for $T_i = 400$ °C) are compared to the behavior of a monolayer electrode prepared in the same conditions. Whatever the electrode microstructure, the experimental electrode impedance diagrams are composed of overlapping contributions, as shown in Fig. 9. First, the electrode characteristics can be interpreted as resulting from two contributions. The magnitudes of which seem to depend on the electrode microstructure. At this stage, no interpretation is proposed to explain the influence of the processing parameters upon the electrode reaction mechanism. The determination of the elementary steps of oxygen reduction is outside the scope of this paper. Nevertheless, the results are interpreted in two dimensions: the high frequency resistance R_{HF} deduced from the high frequency intercept of the electrode characteristic on the real axis (in the Nyquist plane) and, the overpotential resistance R_p calculated from the difference between the dc resistance of the half-cell and R_{HF}. R_p is representative of the electrochemical process involved in the oxygen reduction reaction and thus of the electrochemical performances of the electrode material for a well defined microstructure.

In the case of a monolayer electrode, the resistive contributions are too high compared to what was expected. At 800 °C, these resistances, R_{HF} and R_p, are equal to 80 and $180\,W\,cm^2$, respectively. Regardless of the thickness of the investigated electrodes, the large overpotential resistance may be viewed as resulting from a non-uniform current distribution along the porous electrode/electrolyte interface [28]. Fleig et al. [29] have also demonstrated that the current constriction at the electrode/electrolyte interface can contribute to the low frequency part of the electrolyte impedance

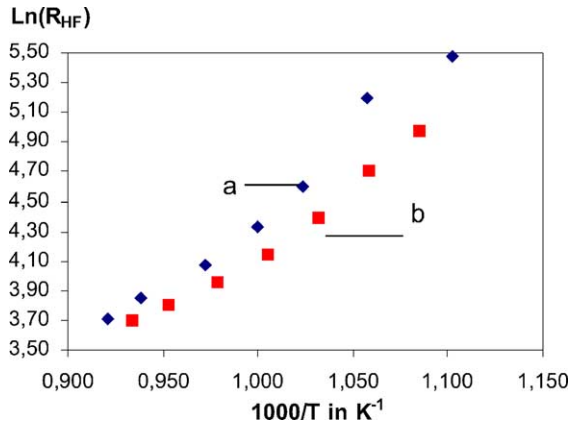

Fig. 10. Temperature dependence of RHF for (a) heating cycle and (b) cooling cycle.

diagram. At least, a part of the additional electrolyte resistance can raise overlap the true electrode impedance and can misleadingly be taken into account in the electrode polarization measurements. It is worth noting that the current constriction resistances are expected to be determined by the electrolyte [30]. In the case of a current constriction at the electrode/electrolyte interface, Sasaki et al. [31] also observed an increase in the measured electrolyte resistance. They related the large cathodic polarization (depending on the microstructure of the electrodes) to a small connection between LSM*x* grains.

The origin of the total ohmic loss in a half-cell is the resistance of both the cathode and the electrolyte. Assuming that the electronic conductivity of the electrode layer is sufficiently high, the ohmic loss in the cathode is negligible in the chosen cell configuration. The temperature dependence of R_{HF} is not exactly similar to that of the YSZ substrate (Fig. 10). For instance, the evolution of the high frequency resistance as a function of temperature is not linear within the studied temperature range. Moreover, a thermal hysteresis is detected during heating and cooling cycles. The results suggest that the large R_{HF} value is not likely to be due to an inhomogeneous current density distribution. In addition, one should consider a term relative to the electrode microstructure. The amplitude and the behavior of the impedance spectra are influenced by the nature of the contact of the current collector with the working electrode (Figs. 9 and 11). The Pt grid current collector gives lower results than the Pt coating. The ohmic and polarization resistance are then lower: $R_{HF} = 1.5\,\Omega\,cm^2$ and $R_p = 1.2\,\Omega\,cm^2$ at 800 °C. The magnitude of the overpotential resistance of LSM-based cathodes still depends on the nature of the current collector [32]. Nevertheless, the frequency distribution of the electrode characteristics does not significantly vary. The evolution of the frequency distribution of the electrode impedance, when the surface coverage of the current collector is changed (Fig. 11), suggests that the improvement of the electrochemical properties of thin films does not originate only from an increasing number of

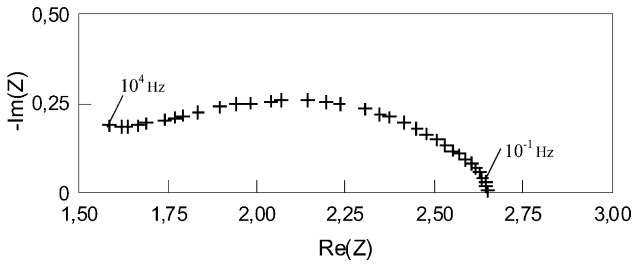

Fig. 11. Impedance diagram of a LSM04 monolayer with Pt coating as current collector.

active reaction sites. In this system, the processes involved in the electrode reaction are different. Whatever the elementary electrochemical steps, these results indicate that the significance of the contact resistances associated with the electrode coating and the current collector is in agreement with previous data [31]. The lower the contact surface area of the current collector, the higher the overpotential resistance. Good electrochemical performances are obtained when the surface of the current collector with the working electrode is the highest. In the case of a Pt grid, the monolayer electrodes have a low transversal electrical conductivity which limits the electrochemical performances. In the recent technology (cross flow, for example), the current collector presents a low contact surface with the cathode. Accordingly, a Pt grid was used to characterize the electrochemical behavior of multilayers.

Fig. 12 shows the impedance spectra for multilayers with $n = 3$ and 5, measured at 800 °C. As it can be seen, for $T_i = 400$ °C, the electrochemical performances of multilayers are higher than the one observed for monolayer with the same strontium content. The evolution of the resistance with the temperature shows that the electrical conduction limits the electrochemical performances. This result agrees with the electrical measurements. The electrical conductivity is higher than the one observed for monolayer. In conclusion, the increase in particles percolation of LSM*x* films allows for an increase in the electrical and the electrochemical performances of the cathode. However, the polarization resistance is still too high for industrial applications.

The influence of T_i on the polarization resistance measured at 800 °C was studied for three layers. The values are

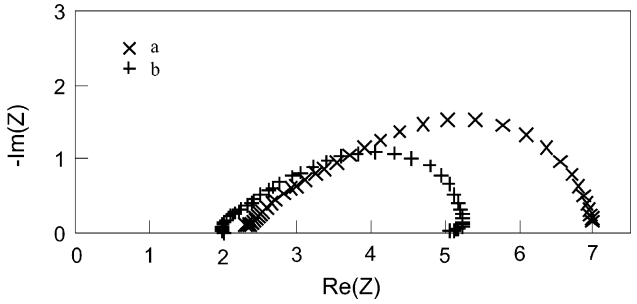

Fig. 12. Impedance diagrams of LSM04 multilayers, with $T_i = 400$ °C, for (a) $n = 3$ and (b) $n = 5$.

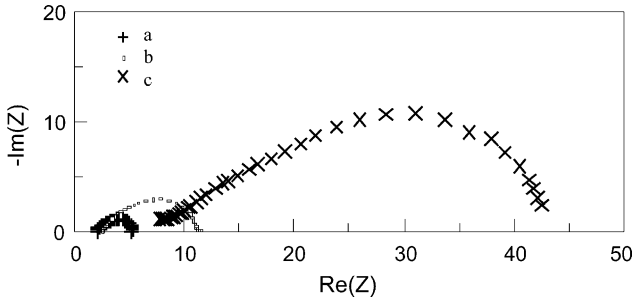

Fig. 13. Impedance diagrams of LSM04 multilayers, with $n = 3$, for (a) $T_i = 400\,^{\circ}C$; (b) $T_i = 1000\,^{\circ}C$; (c) $T_i = 700\,^{\circ}C$.

5, 35 and 9 $W\,cm^2$ for $T_i = 400$, 700 and 1000 °C, respectively. The results are comparable for $T_i = 400$ and 1000 °C. This could be explained by the microstructure. Indeed, the particles size, the porosity and the thickness are very similar for these two intermediate temperatures. However, for $T_i = 700\,^{\circ}C$, an increase in both the ohmic and polarization losses are observed mainly due to a lower porosity. It is worth noting that the ratio of Rp to RHF is nearly the same whatever the microstructure (and thickness) of the film. At 800 °C, the values of the high frequency resistance are 2, 11 and 3 $W\,cm^2$ for $T_i = 400$, 700 and 1000 °C, respectively (Fig. 13). For $T_i = 700\,^{\circ}C$, the resistances R_{HF} are higher than for other T_i, whereas the porosity in this film is the lowest. This result seems to prove that the contact surface area, in this last case (700 °C), is lower than for the other cases (400 and 1000 °C). This fact suggests that the current limit still probably governs the impedance response and that a sufficient percolation of LSM*x* grains is required to decrease both the ohmic and polarization losses. But we can add that the larger polarization resistance (for $T_i = 700\,^{\circ}C$) could also be partly due to a decreasing density of the active reaction sites.

4. Conclusion

The synthesis parameters of LSM*x* films have been studied through a polymeric route. It was clearly demonstrated that the final heating temperature of the films coated on YSZ substrates should not be over 1000 °C. Indeed, above this temperature, formation of $La_2Zr_2O_7$ phase occurs at the film/substrate interface. Multilayers synthesis allowed us to control films thickness. Films morphology have been modified by changing the intermediate calcination temperature (T_i) used in the multilayers synthesis. Three T_i were used. For LSM04 and for $T_i = 400\,^{\circ}C$, the five layers deposit is 34% porous, but is only 15% porous for $T_i = 700\,^{\circ}C$. Whatever T_i, via this polymeric method, thin films were synthetized with thickness ranging from 200 to 1000 nm and with a nanometric grain size distribution. A nanometric grain size distribution when coupled with an important micro-porosity allows for the presence of a high number of active reaction sites.

The films composition, thickness and morphologies were correlated to the electrical and electrochemical properties. The electrical conductivity measurements made on a three layers deposit, with $T_i = 400\,^{\circ}C$, for $x = 0, 0.2$ or 0.4, showed that the most important conductivity is obtained for LSM04. Then, the electrochemical measurements were focused on this composition. Thin films with different thicknesses and morphologies were characterized by impedance spectroscopy. The influence of T_i was studied and the best results were obtained for $T_i = 400\,^{\circ}C$. Next, the influence of the number of layers (n) was studied on films elaborated with $T_i = 400\,^{\circ}C$. Monolayers were shown to present bad electrochemical properties because of their low electrical conductivities. Multilayers, with $n = 3$ or 5, have similar performances. For $T_i = 400$ or 1000 °C, i.e. in case of suitable Pt grid current collector contact, the polarization resistances at 800 °C are about 3–5 $W\,cm^2$. But the point to underline, for such porous layers, is that the current collection process on cathodes surface seems the key parameter for using these cathodes into industrial stacks.

Acknowledgements

Authors thank their colleagues of ICMCB Institute (Bordeaux) for the collaboration in the determination of the cells electrical performances.

References

[1] P. Stevens, F. Novel-Cattin, A. Hammou, C. Lamy, M. Cassir, Les Piles à Combustible, Technique de l'Ingénieur D 5 (2000) 3340.
[2] M.Q. Nguyen, J. Am. Ceram. Soc. 76 (3) (1993) 563.
[3] T. Takeda, R. Kamo, Y. Kawamoto, Y. Takeda, O. Yamamoto, J. Electrochem. Soc. 147 (5) (2000) 1730.
[4] H.S. Yoon, S.W. Choi, D. Lee, B.H. Kim, J. Power Sources 93 (1–2) (2001) 1.
[5] J.J.M. Bae, B.C.H. Steele, Solid State Ionics 106 (1998) 247.
[6] S.P.S. Badwal, S.P. Jiang, J. Love, J. Nowotny, M. Rekas, E.R. Vance, Ceram. Int. 27 (4) (2001) 419.
[7] P. Pechini, Patent 3.330.697 (11 July 1967).
[8] I. Maurin, P. Barboux, J.P. Boilot, Mater. Res. Soc. Symp. Proc. (1997) 453.
[9] M.J. Jorgensen, S. Primdhal, C. Bagger, M. Mogensen, Solid State Ionics 139 (2001) 1.
[10] M.J.L. Ostergard, C. Claussen, C. Bagger, M. Mogensen, Electrochem. Acta 40 (12) (1995) 1971.
[11] S. Wang, Y. Jiang, Y. Zhang, J. Yan, W. Li, J. Electrochem. Soc. 146 (6) (1998) 1932.
[12] F.H. van Heuweln, H.J.M. Bouwmeester, J. Electrochem. Soc. 144 (1) (1997) 134.
[13] M. Gaudon, C. Laberty-Robert, F. Ansart, P. Stevens, A. Rousset, J. New Mater. Electrochem. Syst. 5 (2002) 57.
[14] H. Klug, L. Alexander, X-ray Diffraction Procedures, Wiley, New York, 1962.
[15] M.C. Brant, L. Dessemond, Solid State Ionics 138 (2000) 1.
[16] A. Hammouche, E. Siebert, A. Hammou, M. Kleitz, J. Electrochem. Soc. 138 (5) (1991) 1212.

[17] H. Taimatsu, K. Wada, H. Kaneko, H. Yamamura, J. Am. Ceram. Soc. 75 (1992) 401.
[18] S. De Souza, S.J. Visco, L.C. De Jonghe, J. Electrochem. Soc. 14 (3) (1997).
[19] O. Yamamoto, M. Dokiya, H. Tagawa, Solid oxide fuel cells, in: Proceedings of the 1st International Symposium, SOFC, Japan, 1996.
[20] J.A.M. Van Roosmalen, J.P.P. Huijsmans, L. Plomp, Solid State Ionics 66 (1993) 279.
[21] A. Hammouche, E.J.L. Schouler, M. Henault, Solid State Ionics 2830 (1988) 1205.
[22] S.T. Aruna, M. Muthuraman, K.C. Patil, J. Mater. Chem. 7 (12) (1999) 2499.
[23] T. Tsai, S.A. Barnett, J. Electrochem. Soc. 145 (5) (1998) 1696.
[24] M. Gaudon, C. Laberty-Robert, F. Ansart, P. Stevens, A. Rousset, Solid State Sci. 4 (2002) 125.
[25] I. Maurin, P. Barboux, Y. Lassailly, J.P. Boilot, F. Villain, J. Magnetism Magnetic Mater. 211 (2000) 139.
[26] S. Linderoth, in: A.J. Mc Evoy (Ed.), Proceedings of the 4th European Fuel Cell Forum, Switzerland, 2000, p. 19.
[27] V. Dusastre, J.A. Kilner, Solid State Ionics 126 (1999) 163.
[28] A.M. Svensson, K. Nisciangluu, J. Electrochem. Soc. 145 (9) (1998) 3130.
[29] J. Fleig, P. Pham, P. Sztulzaft, J. Maier, Solid State Ionics 113–115 (1998) 739.
[30] J. Fleig, J. Maier, J. Electrochem. Soc. 144 (11) (1997) 302.
[31] K. Sasaki, J.-P. Wurth, R. Gschwend, M. Gödickemeier, L.J. Gauckler, J. Electrochem. Soc. 143 (2) (1996) 530.
[32] A. Ringuede, J. Fouletier, L. Dessemond, in: A.J. McEvoy (Ed.), Proceedings of the 4th European Solid Oxide Fuel Cell Forum, Switzerland, 2000, p. 283.